Explosive nucleation of superconductivity in a magnetic field

M. Ghinovker
Institute of Superconductivity, Department of Physics, Bar-Ilan University, Ramat Gan 52900, Israel

I. Shapiro
Faculty of Engineering, Tel-Aviv University, Tel-Aviv, 69978, Israel

B. Ya. Shapiro*
Institute of Superconductivity, Department of Physics, Bar-Ilan University, Ramat Gan 52900, Israel
(Received 15 June 1998; revised manuscript received 15 September 1998)

Relaxation dynamics of a normal spot in a magnetic field below the critical temperature is considered. Three different regimes of superconducting nucleation leading to the Abrikosov vortex state are predicted analytically and observed numerically. In particular, a split of supervortex, regular growth of the Abrikosov lattice, and explosive creation of vortex-antivortex liquid are possible scenarios. [S0163-1829(99)07213-6]

I. INTRODUCTION

Since the discovery of high-temperature superconductivity,[1] there has been a growing interest in the magnetic properties of type-II superconductors.[2] Although the thermodynamics of this state is now well investigated, there still remain many unsolved problems concerning its dynamics. In particular, nucleation of the superconducting phase in the presence of an external magnetic field is of great interest due to a variety of possible scenarios.[3–6]

It is well known from the celebrated paper of Abrikosov[7] that in type-II superconductors such a nucleation results in the rise of a mixed state which is characterized by the presence of vortices forming a periodical lattice. Each vortex possesses a topological charge $n=\pm 1$ defined by the $2\pi n$ change of phase χ of the superconducting order parameter $\psi=|\psi|\exp(i\chi)$ around the vortex core. The sign of integer number n distinguishes between vortex and antivortex.

When the normal-to-superconducting phase transition line $H_{c2}(T)$ is crossed slowly comparatively to superconducting nucleation time τ_A, the order parameter grows in the form of an Abrikosov lattice from the very beginning. Such a situation is generic for experiments where a superconductor is cooled slowly in the external magnetic field.

Recently, significant interest has been shown in the situations where superconductivity is restored in the strongly overcooled normal regions appearing, for example, as a result of a short laser pulse applied to the superconductor with magnetic flux inside. Then after the laser radiation is off, a strongly overcooled normal spot exists, provided heat has left this spot for a sufficiently short time $\tau_h \ll \tau_A$.[3]

Another scenario leading to similar overcooled normal spots takes place when topologically multicharged normal spots enter a superconductor from its edge after a sudden increase of the external magnetic field.[8,9] Every such normal spot possesses a topological charge n assigned by trapped magnetic flux and it is conserved throughout the whole future evolution.

Although the final thermodynamical state in all these cases will be some kind of Abrikosov vortex structure, a variety of metastable intermediate states is expected. In particular, n-quanta supervortices and vortex-antivortex mixtures are two principle possibilities.

In the present paper we investigate the problem of superconducting relaxation and vortex formation in normal spots of different sizes in magnetic field. We predict the existence of three different regimes of superconducting nucleation: explosive creation of both vortices and antivortices with conserving total topological charge, regular growth of the Abrikosov lattice, and symmetrical splitting of the supervortex into single vortices.

II. BASIC EQUATIONS

We start with the time-dependent Ginzburg-Landau (TDGL) equations in the form[10–12]

$$\gamma\left(\frac{\partial\Psi}{\partial t'}+2i\frac{e}{\hbar}\mu'\Psi\right)=-\left[a+b|\Psi|^2+\frac{1}{4m}\left(i\hbar\nabla+\frac{2e}{c}\mathbf{A}'\right)^2\right]\Psi+\tilde{f}(\mathbf{r},t), \tag{1}$$

$$\nabla\times\nabla\times\mathbf{A}'=\frac{4\pi}{c}(\sigma\mathbf{E}+\mathbf{J}_s), \tag{2}$$

$$\mathbf{E}=-\frac{1}{c}\frac{\partial\mathbf{A}'}{\partial t'}-\nabla\mu', \tag{3}$$

$$\mathbf{J}_s=-\frac{ie\hbar}{2m}(\Psi^*\nabla\Psi-\Psi\nabla\Psi^*)-\frac{2e^2}{mc}|\Psi|^2\mathbf{A}', \tag{4}$$

$$\nabla\cdot\mathbf{A}'=0. \tag{5}$$

Here $\mathbf{A}'$ and μ' are the vector and scalar potential, respectively; a and b are Ginzburg-Landau coefficients; $\mathbf{E}$ and $\mathbf{J}_s$ are the electric field and supercurrent, respectively, $\tilde{f}$ is the random force due to white thermal noise, σ is normal conductivity; and γ is the phenomenological constant.

These equations should be accompanied by the boundary conditions which have a well-known form, corresponding to the superconductor-insulator contact:

$$\left(-i\hbar\nabla-\frac{2e}{c}\mathbf{A}'\right)_n\Psi=0\,. \tag{6}$$

Assuming local charge neutrality (meaning that the Debye screening length is smaller than the penetration depth), one can eliminate the scalar potential from the TDGL equations, while keeping the relation (5),[13] by the gauge transformation of the potentials

$$\mathbf{A}'\to\mathbf{A}'-\frac{\hbar c}{2e}\nabla\theta;\quad \mu'\to\mu'+\frac{\hbar}{2e}\frac{\partial\theta}{\partial t} \tag{7}$$

accompanied by the shift of the order-parameter phase

$$\Psi\to\Psi\exp(-i\theta) \tag{8}$$

and setting new $\mu'=0$.

It is convenient to define the dimensionless variables as follows:

$$r=r'/\xi,\quad t=t'/\tau_{\mathrm{GL}},\tau_{\mathrm{GL}}\equiv 4\pi\sigma\xi^2/c^2, \tag{9}$$

$$\mathbf{A}=\mathbf{A}'/(\sqrt{2}\,\delta H_{\mathrm{cm}}),\ \ \mathbf{H}=\mathbf{H}'/(\sqrt{2}H_{\mathrm{cm}}),\quad \psi=\Psi/\psi_0,$$

$$f=\tilde{f}\sqrt{\frac{b}{|a|^3}}, \tag{10}$$

where k_B is the Boltzman constant, $\mathbf{H}$ is the dimensionless magnetic field, and

$$\xi=\frac{\hbar}{\sqrt{4m|a|}},\ \ \psi_0=\sqrt{|a|/b},\quad H_{\mathrm{cm}}=\frac{\Phi_0}{\sqrt{8}\pi\xi\delta}. \tag{11}$$

Here ξ is the coherence length, δ is the penetration depth of the magnetic field, H_{cm} is the thermodynamic critical magnetic field, and Φ_0 is the flux quantum.

Thus, we can rewrite the TDGL equations in a dimensionless form:

$$\Gamma\frac{\partial\psi}{\partial t}=\psi-|\psi|^2\psi-(i\nabla+\mathbf{A})^2\psi+f(\mathbf{r},t), \tag{12}$$

$$\frac{\partial\mathbf{A}}{\partial t}=-\nabla\times\nabla\times\mathbf{A}-\frac{i}{2\kappa^2}(\psi^*\nabla\psi-\psi\nabla\psi^*)-\frac{1}{\kappa^2}|\psi|^2\mathbf{A}, \tag{13}$$

$$\nabla\cdot\mathbf{A}=0. \tag{14}$$

Here $\kappa\equiv\delta/\xi$ is the Ginzburg-Landau parameter, $\Gamma=\gamma c^2/(4\pi\sigma\xi^2|a|)$, and the boundary condition for the order parameter is

$$(i\nabla+\mathbf{A})_n\psi=0. \tag{15}$$

For the magnetic field $\mathbf{B}=\nabla\times\mathbf{A}$ we require that the tangential component be continuous.

This set of equations describes a variety of phenomena depending on initial conditions. In particular, relaxation of the normal spot surrounded by a bulk superconductor and containing the integer number of flux quanta $\Phi=n\Phi_0$ develops in two very different ways, depending on the initial size of this spot and the topological charge n.

III. LINEAR STABILITY ANALYSIS

In order to understand superconducting nucleation in the magnetic field we begin by studying the stability of time-independent solutions of Ginzburg-Landau equations. In particular we dwell on such situations as the n-quanta supervortex[14] and the overcooled normal state ($\psi\equiv 0$) in the cylinder of radius R surrounded by the superconductor.

We shall treat both these cases in cylindrical geometry when the supervortex is placed at the origin. For a strongly type-II superconductor ($\kappa\gg 1$) magnetic field H is effectively homogeneous over the region of the order-parameter variation:

$$\mathbf{A}\equiv(A_r,A_\varphi,A_z)=(0;Hr/2;0). \tag{16}$$

In this case the order parameter ψ may be represented in the form:

$$\psi\equiv[F(r)+\eta(r,\varphi,t)]\exp(in\varphi), \tag{17}$$

where $F(r)$ is a time-independent cylindrically symmetric profile of the order parameter. Its azimuthal phase dependence of $\exp(in\varphi)$ reflects the fact that the n flux quanta of the magnetic field are trapped in the normal region; $\eta(r,\varphi,t)$ is the perturbation. The specific shape of $F(r)$ is different for the above-mentioned cases.

Substituting Eq. (17) into Eq. (12) we immediately obtain

$$\Gamma\frac{\partial\eta}{\partial t}=\frac{\partial^2\eta}{\partial r^2}+\frac{1}{r}\frac{\partial\eta}{\partial r}+\frac{1}{r^2}\frac{\partial^2\eta}{\partial\varphi^2}+\frac{2in}{r^2}\frac{\partial\eta}{\partial\varphi}-iH\frac{\partial\eta}{\partial\varphi}+\left[1+nH-\frac{H^2r^2}{4}-\frac{n^2}{r^2}-2F^2\right]\eta-F^2\eta^*+\tilde{\xi}. \tag{18}$$

Introducing the real and imaginary parts of the perturbation $\eta=a+ib$, we get the set of two real equations:

$$\Gamma\frac{\partial}{\partial t}a=[\widehat{L^0}-3F^2(r)]a+\left(H-\frac{2n}{r^2}\right)\frac{\partial}{\partial\varphi}b+\tilde{\xi}_r, \tag{19}$$

$$\Gamma\frac{\partial}{\partial t}b=[\widehat{L^0}-F^2(r)]b-\left(H-\frac{2n}{r^2}\right)\frac{\partial}{\partial\varphi}a+\tilde{\xi}_i, \tag{20}$$

where the operator

$$\widehat{L^0}\equiv\frac{\partial^2}{\partial r^2}+\frac{1}{r}\frac{\partial}{\partial r}+\frac{1}{r^2}\frac{\partial^2}{\partial\varphi^2}+1+nH-\frac{H^2r^2}{4}-\frac{n^2}{r^2}. \tag{21}$$

Expanding a and b in Fourier series:

$$a=\frac{C_0}{2}+\sum_{m=1}^{\infty}(C_m\cos m\varphi+D_m\sin m\varphi), \tag{22}$$

$$b=\frac{P_0}{2}+\sum_{k=1}^{\infty}(P_m\cos m\varphi+Q_m\sin m\varphi), \tag{23}$$

and substituting into Eqs. (19), (20) we get the following set of equations for Fourier amplitudes:

$$\Gamma\frac{\partial}{\partial t}C_0=\widehat{L_m}C_0-3F^2(r)C_0;\ \ \Gamma\frac{\partial}{\partial t}P_0=\widehat{L_m}P_0-F^2(r)P_0 \tag{24}$$

and

$$\Gamma\frac{\partial}{\partial t}C_m=\widehat{L_m}C_m-3F^2(r)C_m+\left(H-\frac{2n}{r^2}\right)mQ_m, \tag{25}$$

$$\Gamma\frac{\partial}{\partial t}D_m=\widehat{L_m}D_m-3F^2(r)D_m-\left(H-\frac{2n}{r^2}\right)mP_m, \tag{26}$$

$$\Gamma\frac{\partial}{\partial t}P_m=\widehat{L_m}P_m-F^2(r)P_m-\left(H-\frac{2n}{r^2}\right)mD_m, \tag{27}$$

$$\Gamma\frac{\partial}{\partial t}Q_m=\widehat{L_m}Q_m-F^2(r)Q_m+\left(H-\frac{2n}{r^2}\right)mC_m, \tag{28}$$

where

$$\widehat{L_m}\equiv\frac{\partial^2}{\partial r^2}+\frac{1}{r}\frac{\partial}{\partial r}-\frac{(m^2+n^2)}{r^2}-\frac{H^2r^2}{4}+nH+1. \tag{29}$$

Looking for the solution in the form

$$\begin{pmatrix}C_m(r,t)\\D_m(r,t)\\P_m(r,t)\\Q_m(r,t)\end{pmatrix}=\begin{pmatrix}C_m(r)\\D_m(r)\\P_m(r)\\Q_m(r)\end{pmatrix}\exp\Lambda t, \tag{30}$$

and denoting $\lambda\equiv\Gamma\Lambda$ we obtain

$$[\widehat{L_m}-3F^2(r)]C_m+\left(H-\frac{2n}{r^2}\right)mQ_m=\lambda C_m,$$

$$[\widehat{L_m}-F^2(r)]Q_m+\left(H-\frac{2n}{r^2}\right)mC_m=\lambda Q_m, \tag{31}$$

$$[\widehat{L_m}-3F^2(r)]D_m-\left(H-\frac{2n}{r^2}\right)mP_m=\lambda D_m,$$

$$[\widehat{L_m}-F^2(r)]P_m-\left(H-\frac{2n}{r^2}\right)mD_m=\lambda P_m. \tag{32}$$

We have to find the eigenvalues $\{\lambda\}$ of this problem. All the eigenvalues are real because the system is Hermitian. In the framework of the linear stability analysis we are looking for the parameter values when the greatest eigenvalue crosses zero $\lambda_{\max}=0$. Then it is exactly the point when the solution $F(r)\exp(in\varphi)$ loses its azimuthal stability. The following quantities play roles of parameters for our analysis: unperturbed profile $F(r)$, homogeneous magnetic-field magnitude H, topological charge n. This approach also determines the number m of most unstable harmonics.

The eigenfunctions of this problem (for all $m\neq0$) must vanish at $r=0$ and decay exponentially in the surrounding bulk superconductor when $r\to\infty$. We have solved this eigenvalue problem numerically by discretizing our coordinate space and, therefore, transforming the ordinary differential equation problem to an algebraic one.

The specific character of instability depends essentially on unperturbed profile $F(r)$. In particular for supervortices with $n=1,2,3,4$ we used $F^2(r)\equiv F_n^2(r)$ in the form[15]

$$F_1^2(r)=r^2\frac{0.34+0.07r^2}{1+0.41r^2+0.07r^4}, \tag{33}$$

$$F_2^2(r)=r^4\frac{0.02344+5053r^2}{1+252\,537r^2+20\,212.023r^4+5053r^6}, \tag{34}$$

$$F_3^2(r)=r^6\frac{0.000\,685\,608\,38+r^2}{1+2233.6r^2+122.57r^4+8.999\,314\,39r^6+r^8}, \tag{35}$$

$$F_4^2(r)=r^8\frac{0.000\,011\,072\,650\,76+r^2}{1+31\,735r^2+17\,232.2r^4+192.85r^6+15.999\,988\,927\,34r^8+r^{10}}. \tag{36}$$

In the case of an extended normal area surrounded by a superconductor, the exact shape of $F(r)$ becomes unimportant and it can be well approximated by a step function:[14]

$$F^2(r)=\begin{cases}0 & \text{for } r\leqslant R,\\ 1 & \text{for } r>R,\end{cases} \tag{37}$$

where R is the radius of the normal domain.

Obviously the instability is suppressed by the magnetic field. Calculating $\lambda_{\max}$ for different magnetic-field values H and harmonics m, we are looking for the onset of instability $\lambda_{\max}(H,m)=0$.

This dependence for supervortex with $n=4$ is presented

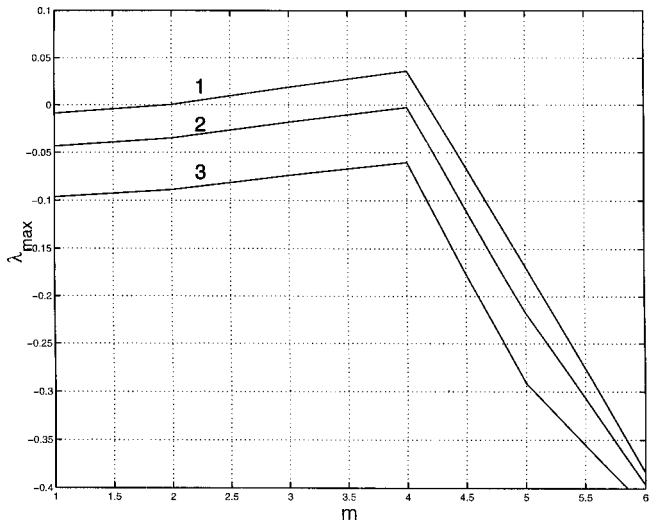

FIG. 1. Rate growth $\lambda_{\max}$ of azimuthal instability for supervortex with the topological charge $n=4$ as a function of the harmonics number m for different magnitudes of magnetic field: (1) $H/H_{\rm cm}=0.95$; (2) $H/H_{\rm cm}=0.99$; (3) $H/H_{\rm cm}=1.05$.

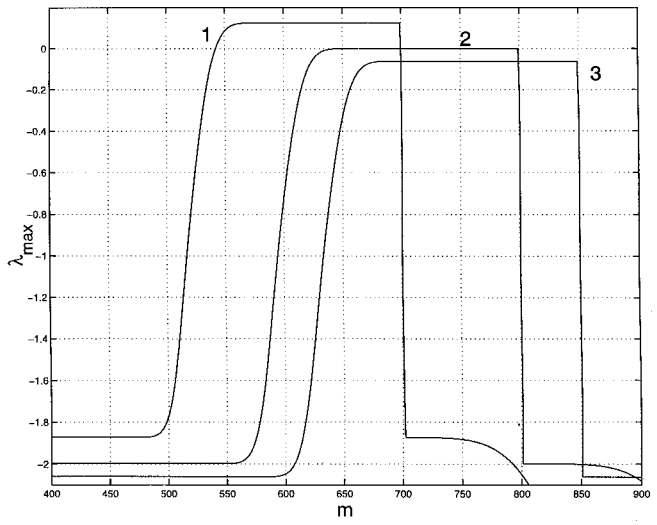

FIG. 3. Rate growth $\lambda_{\max}(m)$ in the large normal spot (of radius $R=40$) for different magnitudes of magnetic field: (1) $H=0.875H_{c2}$ $(n=700)$; (2) $H\equiv H_{\rm onset}=H_{c2}$ $(n=800)$; (3) $H=1.063H_{c2}$ $(n=850)$. Wide band of harmonics becomes unstable simultaneously.

in Fig. 1. The only unstable harmonic here has $m=n$ corresponding to supervortex splitting into n single quantum vortices on the later nonlinear stages of evolution. This instability arises for sufficiently weak magnetic field $H<H_4\approx 0.9H_{\rm cm}$, where H_n is the magnetic field of the instability onset for n charged supervortex. The dependence of rate growth $\lambda_{\max}(m)$ for the supervortex charge $n=1,2,3,4$ and the corresponding H_n is shown in Fig. 2. As was expected, a single quantum vortex is absolutely stable.

The picture looks very different for the instability onset in the large normal domain. In this case the wide spectrum of azimuthal harmonics becomes unstable simultaneously (Fig. 3). (We assumed for simplicity the following relation between the field magnitude, the number of flux quanta in the normal spot, and its radius: $\pi R^2 H=n\Phi_0$). In the limit of an infinitely large normal region this spectrum becomes extremely wide, manifesting the creation of an Abrikosov vortex liquid. The critical magnetic field of the instability onset $H_{\rm onset}$ approaches H_{c2}.

When the magnetic field is below H_{c2}, the rate growth $\lambda_{\max}>0$ for a wide band of harmonics m and this state is sufficiently unstable.

In the opposite case of smaller sizes of normal domain the rate growth curve sharpens (Fig. 4) approaching that found for supervortices, and onset field $H_{\rm onset}$ decreases to about $H_{\rm cm}$. Such crossover behavior for different spot sizes is shown in Fig. 5. Thus, two different types of instability may arise for large and small normal spots ($R\lesseqgtr R_{\rm cr}$).

In accordance with this linear stability analysis the supervortex with $n>1$ is unstable. However, this instability occurs at magnetic field $H\sim H_{\rm cm}$ which is sufficiently higher

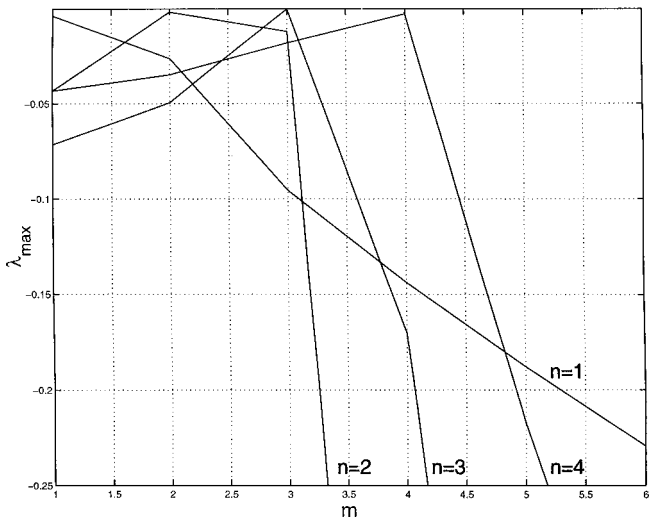

FIG. 2. Rate growth $\lambda_{\max}(m)$ for the supervortex charge $n=2,3,4$ for onset magnetic field $H_n:H_2/H_{\rm cm}=0.62$; $H_3/H_{\rm cm}=0.93$; $H_4/H_{\rm cm}=0.99$. For $n=1$ there is no instability [$\lambda_{\max}(m)$ is plotted for $H=0$.]

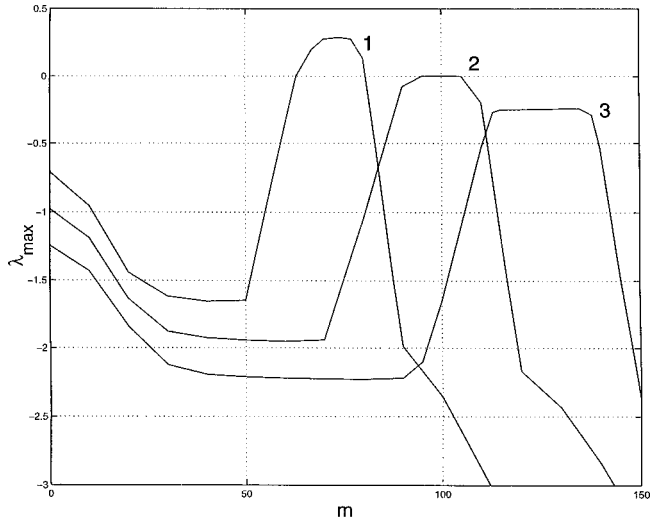

FIG. 4. Rate growth $\lambda_{\max}(m)$ in the normal spot of radius $R=15$ for different magnitudes of magnetic field: (1) $H=0.711H_{c2}$ $(n=80)$; (2) $H\equiv H_{\rm onset}=0.996H_{c2}$ $(n=112)$; (3) $H=1.244H_{c2}$ $(n=140)$.

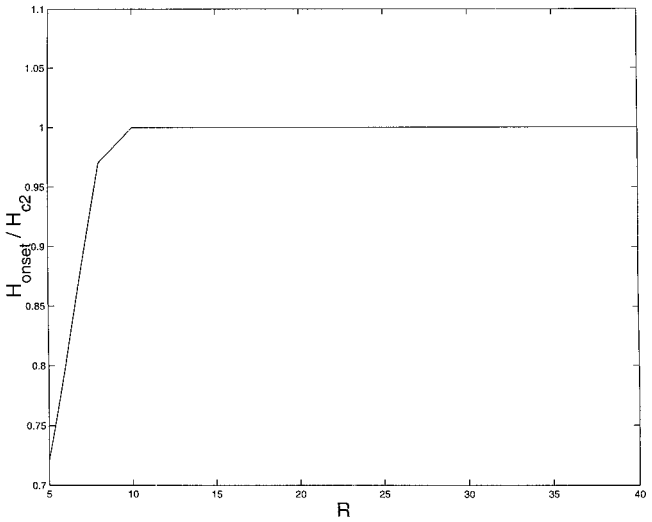

FIG. 5. The instability onset magnetic field $H_{\rm onset}$ versus the normal spot radius R.

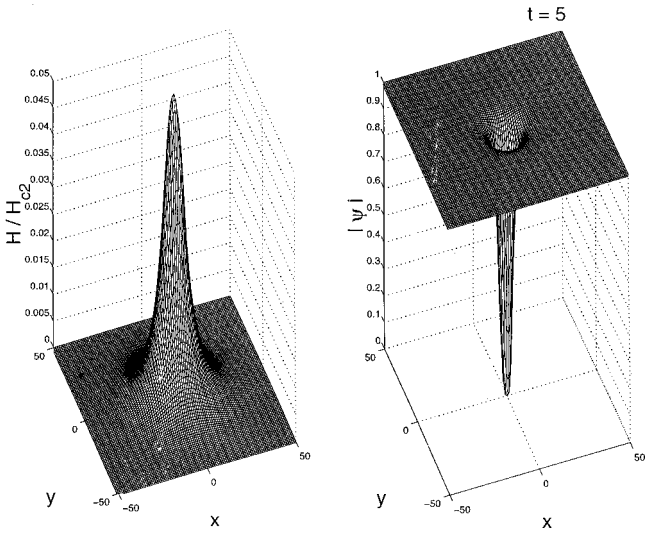

FIG. 6. Magnetic-field magnitude H and order-parameter absolute value $|\psi|$ profiles at $t=5$ for $n=4$, $\kappa=10$, $\Gamma=1$, and thermal noise $|f|<0.001$, for initially small normal spot (radius $R=2$).

than the field in the supervortex center $H_p \approx 2H_{c1}$, where H_{c1} is the lower critical magnetic field. In the large normal domain the instability develops just below the upper critical field H_{c2}. For smaller radius the instability arises at lower magnetic field tending to $H \sim H_{\rm cm}$ for sizes of supervortex order.

IV. EXACT NONLINEAR DYNAMICS

It is clear that these two types of linear instability must result in the formation of very different patterns on nonlinear stages of evolution. In order to study nonlinear dynamics in full detail the TDGL equations (12)–(14) have been solved numerically. This dynamics depends on initial conditions which in our case were chosen in the form:

$$\chi(\mathbf{r},t=0)=n\varphi, \tag{38}$$

$$|\psi(\mathbf{r},t=0)|=\begin{cases} 0; & r<R-1 \\ (r+1-R); & R-1<r<R, \\ 1; & r>R \end{cases} \tag{39}$$

$$A=\{A_r;A_\varphi\}; \quad A_r(\mathbf{r},t=0)\equiv 0, \tag{40}$$

$$A_\varphi(\mathbf{r},t=0)=\begin{cases} (H_0/2)r; & r<R, \\ -H_0\kappa(K_1(r/\kappa)/K_0(R/\kappa))+n/r; & r>R, \end{cases} \tag{41}$$

where

$$H_0 \equiv \frac{(n/R)K_0(R/\kappa)}{\kappa K_1(R/\kappa)+(R/2)K_0(R/\kappa)}. \tag{42}$$

Here K_0 and K_1 are the modified Bessel functions.

Thus, initially, we have a normal spot ($|\psi|=0$) of radius R with n quanta of magnetic field trapped inside ($\Phi_0=2\pi\kappa$ in dimensionless units). The phase of the order parameter χ increases linearly to provide the total topological charge n. The magnetic field is uniform across the spot and decays outside.[16]

We solved these equations in the square domain (250×250). The magnetic field at the sample edges is assumed to be zero. Two different boundary conditions for the order parameter were imposed—that given by Eq. (15) and the simplified conditions:[6]

$$(\mathbf{A}(t))_{\rm boundary}=(\mathbf{A}(0))_{\rm boundary}, \quad \left(\frac{\partial\psi}{\partial\mathbf{n}}\right)_{\rm boundary}=0. \tag{43}$$

The dynamics far from the boundaries was found to be independent of the type of boundary conditions.

In our computations with the latter boundary conditions we have used the simple ''alternating-direction'' implicit scheme of forward and backward sweeps on a discretized rectangular grid (cf. Ref. 17). The parameters in the calculations described below were set as follows: $\Gamma=1$, $\eta(\mathbf{r},t)$ was uniformly distributed in the segment $|\eta|\leqslant 0.001$ random function.

For the boundary condition (15) the link variable approach has been applied. This computational technique is presented in the Appendix.

The results of numerical simulation are presented in Figs. 6–11. In fact, two distinct scenarios of evolution take place. In particular, when the initial magnetic field exceeds H_{c2}, a normal spot grows at the beginning and magnetic field inside decreases (Fig. 6). When the magnetic field levels with H_{c2}, a superconducting phase arises in the spot. Later, in magnetic field close to $H_{\rm cm}$ azimuthal instability appears, splitting the multiquantum state into single vortices (Fig. 7).

In the opposite case when the initial magnetic field is much weaker than $H_{\rm cm}$ the normal spot shrinks rapidly (Fig. 8) and simultaneously superconductivity appears all over the normal spot. This superconducting phase cannot grow uniformly because of the magnetic field suppressing order parameter in some points with topological charge P_i. Generically, the number of such zeros of the order parameter equals the total topological charge n. However, due to a spatial degeneracy of the order parameter many more zeroes are created—separated roughly by ξ. The conservation of the topological charge requires that part of these zeroes are charged negatively and $\Sigma P_i=n$. In evolution this process

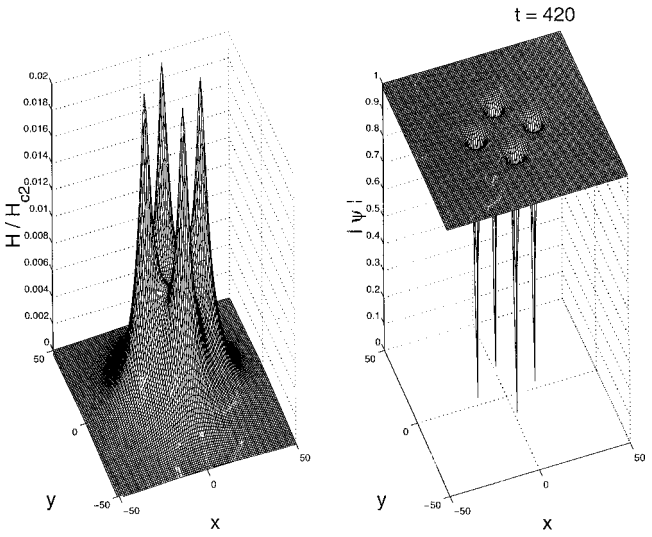

FIG. 7. Split of four-quanta supervortex shown in Fig. 6 into single vortices for $t=420$.

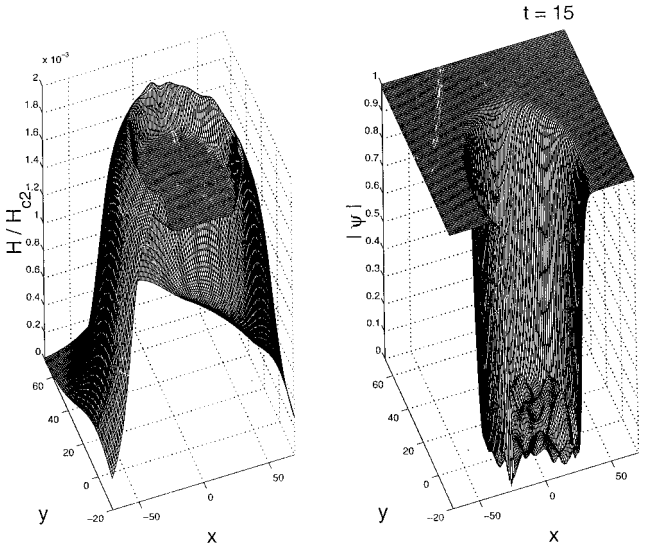

FIG. 9. Onset of explosive vortex-antivortex nucleation inside the normal spot shown in Fig. 8 for $t=15$.

looks like a topological explosion (Fig. 9). In further dynamics, in spite of massive annihilation of adjacent zeroes of opposite sign, the remaining zeros will grow into Abrikosov vortices and antivortices forming a metastable phase (Fig. 10). Eventually only n vortices will survive (Fig. 11).

V. CONCLUSION

One can conclude that depending on the initial overcooled normal state there exist three different regimes of nucleation leading to setting up the Abrikosov vortex state in a sample. Namely, if an initially strong magnetic field ($H>H_{c2}$) is confined in a small normal spot of size $R\geqslant\xi$, the order parameter evolves towards the supervortex profile splitting into single vortices (Fig. 7). This process is similar to a well-known supervortex decay in the liquid helium.[15]

In an initially large normal domain ($R\gg\xi$) there are two possible scenarios. When magnetic field in the region reaches H_{c2} from above, the order parameter grows leaving a regular lattice of zeros. Subsequently, this state develops to a usual Abrikosov vortex lattice with a separation $\sim\xi$ between vortex cores (Fig. 12).

The most intriguing behavior appears when magnetic field in the spot is relatively weak ($H\ll H_{c2}$) in the initial state. This state is strongly unstable [rate growth $\lambda_{\max}(H,m)>0$] from the very beginning. Superconductivity arises creating again a set of the order-parameter zeros separated by the distance $\sim\xi$. However, in a weak magnetic field the density of these zeros exceeds considerably the mean number of flux quanta per unit area, which means that this set contains not only vortices but also antivortices. Most of the vortex-antivortex pairs annihilate rapidly. Nevertheless some antivortices may survive, resulting in long-living metastable vortex-antivortex liquid (Fig. 13).

Let us discuss the characteristic time scales of overcooled spot evolution. Immediately after heat relaxation $t\geqslant\tau_h$

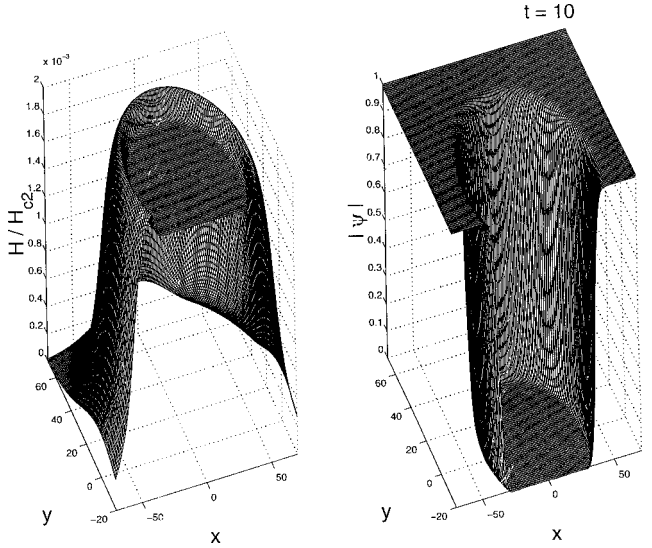

FIG. 8. Magnetic-field magnitude H and order-parameter absolute value $|\psi|$ profiles at $t=10$ for $n=4$, $\kappa=10$, $\Gamma=1$, and thermal noise $|f|<0.001$, for large initial normal spot ($R=55$).

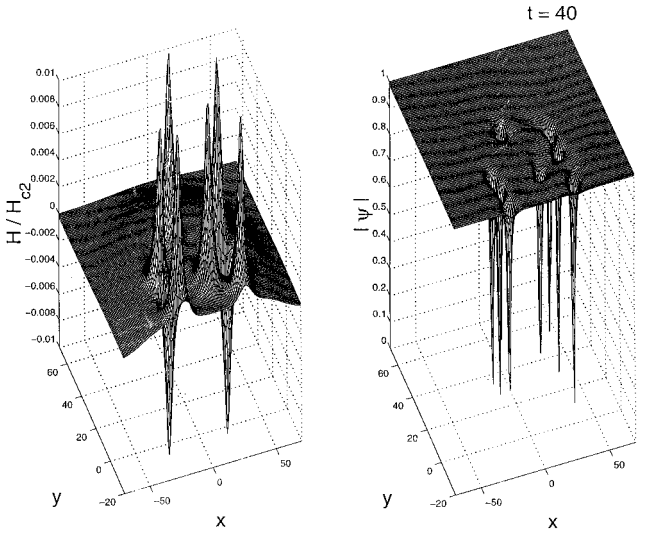

FIG. 10. Metastable vortex-antivortex mixture consisting of six vortices and two antivortices as a further stage of evolution shown in Figs. 8, 9 for $t=40$.

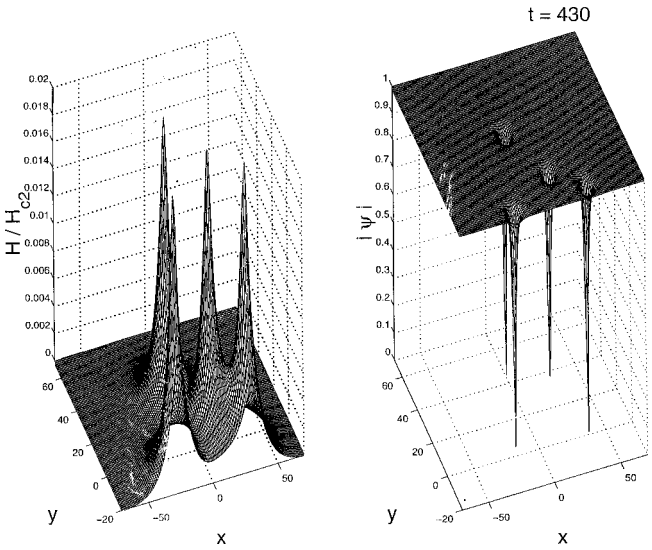

FIG. 11. Final stage of evolution (see Figs. 8–10) for $t=430$.

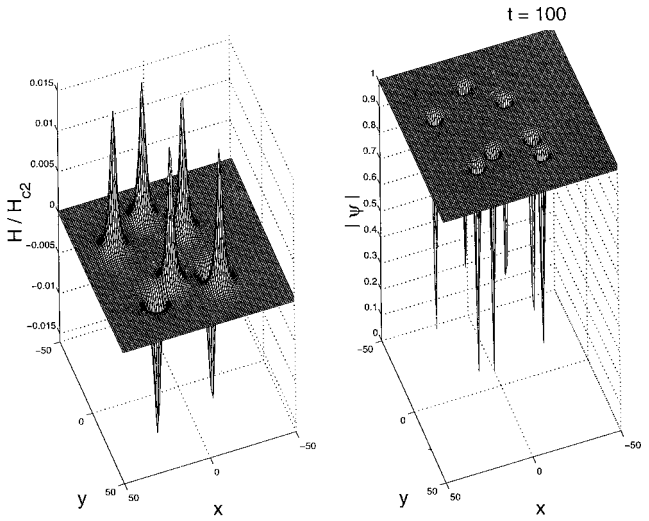

FIG. 13. Magnetic-field magnitude H and order-parameter absolute value $|\psi|$ profiles for the metastable vortex-antivortex state at $t=100$ for $n=3$, $\kappa=10$, $\Gamma=5.79$, and thermal noise $|f|<0.1$. Initial normal spot was of radius $R=55$.

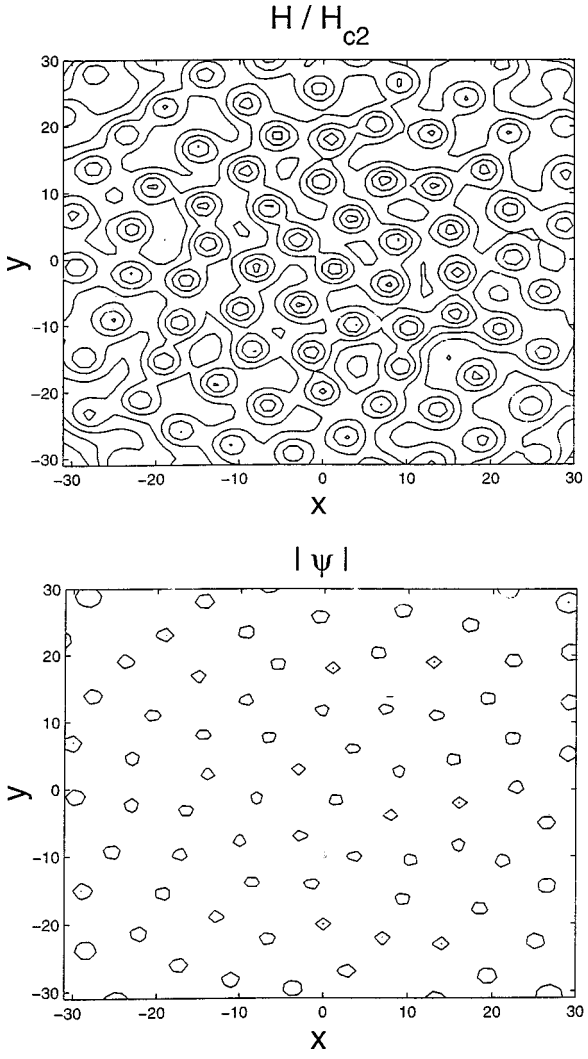

FIG. 12. Abrikosov mixed-state creation in the spot with large magnetic flux. Magnetic-field magnitude H and order-parameter absolute value $|\psi|$ contour plots at $t=155$ with $\kappa=10$, $\Gamma=1$. Initial normal spot of radius $R=55$ contained magnetic flux $300\Phi_0$.

$\sim\tau_{GL}\approx 10^{-12}$ s, the strongly nonequilibrium overcooled normal spot starts to relax. At the first stage ($t\leqslant 10\tau_{GL}$) only spot walls motion takes place. At the next stage ($10\tau_{GL}\leqslant t\leqslant 50\tau_{GL}$) explosive nucleation across the spot begins, resulting in the vortex-antivortex mixture. This metastable state may survive for a long time, up to several hundred τ_{GL}, relaxing eventually to the thermodynamical Abrikosov mixed state. However, pinning centers trapping the vortices in the long-living vortex-antivortex mixture phase may prevent their annihilation, freezing such a state for an infinitely long period of time.

ACKNOWLEDGMENTS

We are grateful to I. Aranson, P. Esquinazi, and Y. Yeshurun for their attention and to I. Freund and V. Kogan for fruitful discussions. We would also like to thank the Israel Academy of Sciences and Bar-Ilan Minerva Center for Superconductivity for permanent support and the Inter-University Computational Center for providing Cray J932 supercomputer facilities.

APPENDIX

In our calculations with the boundary condition (15) we exploit the so-called ''link variable'' method[18,19,5] for the discretization of the TDGL equations (12)–(14).

The square spatial domain $\{x\in[-L;L]\}\times\{y\in[-L;L]\}$ is discretized as follows ($a=L/N$):

$$x_k=ka,\ \ y_j=ja;\ \ k,j=-N,-N+1,\ldots,N. \quad \text{(A1)}$$

Then the order parameter is defined on this grid: $\varphi_{k,j}\equiv\Psi(x_k,y_j)$.

We define the components of the vector potential on the ''links'' connecting two adjacent points of the grid:

$$A_x^{k,j}\equiv A_x(x_k+a/2,y_j);\ \ A_y^{k,j}\equiv A_y(x_k,y_j+a/2). \quad \text{(A2)}$$

Next we define the link variables U and V as follows:

$$U_{k,j} \equiv \exp(-iaA_x^{k,j}); \quad V_{k,j} \equiv \exp(-iaA_y^{k,j}). \tag{A3}$$

Finally, in these new variables, our equations become

$$\Gamma \frac{\partial \psi_{k,j}}{\partial t} = \frac{1}{a^2}[\psi_{k+1,j}U_{k,j} + \psi_{k-1,j}U_{k-1,j}^* + \psi_{k,j+1}V_{k,j} + \psi_{k,j-1}V_{k,j-1}^* - 4\psi_{k,j}] + \psi_{k,j} - |\psi_{k,j}|^2\psi_{k,j}, \tag{A4}$$

for $k,j = -N+1, -N+2, \ldots, N-1$,

$$\frac{\partial U_{k,j}}{\partial t} = U_{k,j}\left\{ -\frac{i}{\kappa^2}\mathrm{Im}[\psi_{k,j}^*\psi_{k+1,j}U_{k,j}] - \frac{1}{a^2}[U_{k,j}V_{k+1,j}U_{k,j+1}^*V_{k,j}^*U_{k,j}V_{k+1,j-1}^*U_{k,j-1}^*V_{k,j-1} - 1]\right\}, \tag{A5}$$

for $k = -N, -N+1, \ldots, N-1$, $j = -N+1, -N+2, \ldots, N-1$,

$$\frac{\partial V_{k,j}}{\partial t} = V_{k,j}\left\{ -\frac{i}{\kappa^2}\mathrm{Im}[\psi_{k,j}^*\psi_{k,j+1}V_{k,j}] - \frac{1}{a^2}[V_{k,j}U_{k,j+1}V_{k+1,j}^*U_{k,j}^*V_{k,j}U_{k-1,j+1}^*V_{k-1,j}^*U_{k-1,j} - 1]\right\}, \tag{A6}$$

for $j = -N, -N+1, \ldots, N-1$, $k = -N+1, -N+2, \ldots, N-1$.

The boundary conditions (15) and $(\nabla \times \mathbf{A})_{\text{boundary}} = B_{\text{ext}}$ in this representation read

$$\psi_{-N,j} = U_{-N,j}\psi_{-N+1,j} \quad \text{for } j = -N, -N+1, \ldots, N, \tag{A7}$$

$$\psi_{N,j} = U_{N-1,j}^*\psi_{N-1,j} \quad \text{for } j = -N, -N+1, \ldots, N, \tag{A8}$$

$$\psi_{k,-N} = V_{k,-N}\psi_{k,-N+1} \quad \text{for } k = -N, -N+1, \ldots, N, \tag{A9}$$

$$\psi_{k,N} = V_{k,N-1}^*\psi_{k,N-1} \quad \text{for } k = -N, -N+1, \ldots, N, \tag{A10}$$

$$V_{-N,j} = (1 + ia^2B_{\text{ext}})U_{-N,j+1}^*U_{-N,j}V_{-N+1j}, \quad \text{for } j = -N, -N+1, \ldots, N-1, \tag{A11}$$

$$V_{N,j} = (1 - ia^2B_{\text{ext}})U_{N-1,j}^*U_{N-1,j+1}V_{N-1,j} \quad \text{for } j = -N, -N+1, \ldots, N-1, \tag{A12}$$

$$U_{k,-N} = (1 - ia^2B_{\text{ext}})V_{k+1,-N}^*V_{k,-N}U_{k,-N+1} \quad \text{for } k = -N, -N+1, \ldots, N-1, \tag{A13}$$

$$U_{k,N} = (1 + ia^2B_{\text{ext}})V_{k+1,N-1}^*V_{k,N-1}U_{k,N-1} \quad \text{for } k = -N, -N+1, \ldots, N-1. \tag{A14}$$

This set of equations has been solved numerically on a Cray J932 supercomputer with the time step $\Delta t = 0.001$. For the order parameter equation (A4) the simple ''alternating-direction'' implicit scheme of forward and backward sweeps has been used. For Eqs. (A5), (A6) we have applied the Crank-Nicolson approach (see, for example, Ref. 20).

*Author to whom correspondence should be addressed.

[1] J. G. Bednorz and K. A. Müller, Z. Phys. B **64**, 189 (1986).

[2] Y. Yeshurun, A. P. Malozemoff, and A. Shaulov, Rev. Mod. Phys. **68**, 911 (1996).

[3] P. Leiderer, J. Boneberg, P. Brüll, V. Bujok, and S. Herminghaus, Phys. Rev. Lett. **71**, 2646 (1993); V. Bujok, P. Brüll, J. Boneberg, S. Herminghaus, and P. Leiderer, Appl. Phys. Lett. **63**, 412 (1993).

[4] R. Kato, Y. Enomoto, and S. Maekawa, Phys. Rev. B **44**, 6916 (1991).

[5] R. Kato, Y. Enomoto, and S. Maekawa, Phys. Rev. B **47**, 8016 (1993); R. Kato, Y. Enomoto, and S. Maekawa, Physica C **227**, 387 (1994).

[6] F. Liu, M. Mondello, and N. Goldenfeld, Phys. Rev. Lett. **66**, 3071 (1991).

[7] A. A. Abrikosov, Zh. Eksp. Teor. Fiz. **32**, 1442 (1957) [Sov. Phys. JETP **5**, 1174 (1957)].

[8] I. B. Aranson, M. Gitterman, and B. Ya. Shapiro, Phys. Rev. B **51**, 3092 (1995).

[9] I. Aranson, B. Ya. Shapiro, and V. Vinokur, Phys. Rev. Lett. **76**, 142 (1996).

[10] L. Kramer and R. J. Watts-Tobin, Phys. Rev. Lett. **40**, 1041 (1978).

[11] R. J. Watts-Tobin, Y. Krähenbühl, and L. Kramer, J. Low Temp. Phys. **42**, 459 (1981).

[12] L. P. Gor'kov and G. M. Eliashberg, Zh. Eksp. Teor. Fiz. **56**, 1297 (1969) [Sov. Phys. JETP **29**, 698 (1969)].

[13] N. R. Werthamer, in *Superconductivity*, edited by R. D. Parks (Marcel Dekker, New York, 1969).

[14] D. Saint-James, G. Sarma, and E. J. Thomas, *Type-II Superconductivity* (Pergamon, New York, 1969.

[15] I. Aranson and V. Steinberg, Phys. Rev. B **53**, 75 (1996).

[16] G. S. Mkrtchyan and V. V. Shmidt, Zh. Eksp. Teor. Fiz. **61**, 367 (1971) [Sov. Phys. JETP **34**, 195 (1972)].

[17] S. E. Koonin and D. C. Meredith, *Computational Physics* (Addison-Wesley, Reading, MA, 1990).

[18] S. L. Alder and T. Piran, Rev. Mod. Phys. **56**, 1 (1984).

[19] E. Coskun and M. K. Kwong, Nonlinearity **10**, 579 (1997).

[20] D. Greenspan, *Discrete Numerical Methods in Physics and Engineering* (Academic, New York, 1974).